Link-usage asymmetry and collective patterns emerging from rich-club organization of complex networks

Paolo Moretti[a,1] **and Marc-Thorsten Hütt**[b]

[a]Institute of Materials Simulation, Department of Materials Science, Friedrich-Alexander-University Erlangen-Nürnberg, D-90762 Fürth, Germany; and [b]Department of Life Sciences and Chemistry, Jacobs University Bremen, D-28759 Bremen, Germany

Edited by Terrence J. Sejnowski, Salk Institute for Biological Studies, La Jolla, CA, and approved June 18, 2020 (received for review November 11, 2019)

In models of excitable dynamics on graphs, excitations can travel in both directions of an undirected link. However, as a striking interplay of dynamics and network topology, excitations often establish a directional preference. Some of these cases of "link-usage asymmetry" are local in nature and can be mechanistically understood, for instance, from the degree gradient of a link (i.e., the difference in node degrees at both ends of the link). Other contributions to the link-usage asymmetry are instead, as we show, self-organized in nature, and strictly nonlocal. This is the case for excitation waves, where the preferential propagation of excitations along a link depends on its orientation with respect to a hub acting as a source, even if the link in question is several steps away from the hub itself. Here, we identify and quantify the contribution of such self-organized patterns to link-usage asymmetry and show that they extend to ranges significantly longer than those ascribed to local patterns. We introduce a topological characterization, the hub-set-orientation prevalence of a link, which indicates its average orientation with respect to the hubs of a graph. Our numerical results show that the hub-set-orientation prevalence of a link strongly correlates with the preferential usage of the link in the direction of propagation away from the hub core of the graph. Our methodology is embedding-agnostic and allows for the measurement of wave signals and the sizes of the cores from which they originate.

excitable media | networks | collective patterns

The relationship between structure and function represents one of the current conceptual hotspots of network theory (1–5) and some of its most relevant applications (6–9). While the structure-vs.-function debate was originated, at least using this denomination, in the context of computational neuroscience, the ability to predict dynamic patterns starting from topological considerations has been for almost two decades among the aims of network models for epidemiology, social sciences, transportation infrastructures, and information systems, to name just a few (10–12).

For two decades, statistical physics has been the core discipline contributing to the development of minimal models of graphs with specific statistical properties, novel characterizations of network topology, and fundamental relationships between network architecture and dynamics (1, 13–16). This has led to a productive dialogue with a range of disciplines, where network concepts have been instrumental in unraveling some organizational principles of the respective systems. Examples range from systems biology and social sciences to manufacturing and neuroscience.

In neuroscience, a wide range of investigations explores the interplay of network topology and excitable dynamics. Two research foci are particularly prominent: 1) the study of correlations between structural connectivity (i.e., the brain network, or connectome) and functional connectivity (derived from excitation patterns) (17–21); and 2) the search for network mechanisms responsible for self-sustained activity (i.e., for amplifying and maintaining excitations) (22–25). In particular, the prominence of the so-called rich-club organization in brain networks has been variously invoked as a key factor in both of the above contexts. By rich club, we refer to a limited set of nodes which, by virtue of their enhanced connectivity or more broadly defined centrality, play a systematic and predictable role in the initiation and development of functional activity patterns. The rich-club organization of brain networks has first been observed in the cortical area network of the cat (26) and is known to play an important role in the global information integration in the human connectome (27). Changes in rich-club organization have been identified in schizophrenia (28) and Alzheimer's disease (29, 30), as well as several other pathologies (31, 32). This localized topological structure—a small set of interconnected nodes with high connectivity and centrality—is thus hypothesized to be of relevance to the dynamical function of the network.

Here, we provide evidence that, even in simple network models, such a localized set can have global dynamical implications. We show that a global, self-organized excitation pattern can be predicted locally from a limited set of nodes, the source or hub set, via the asymmetric usage of links throughout the network.

With their work on reaction-diffusion systems on graphs, Nakao and Mikhailov (33) have drawn the attention to the

Significance

How classical spatiotemporal patterns can be detected and studied in networks is an open question of relevance to brain dynamics, epidemic diseases, and information spreading. Our work fills this conceptual gap, highlighting how propagation patterns in networks with highly connected hubs can be identified by recording local asymmetries in excitation phenomena and predicted by quantifying local orientations with respect to the major emitter hubs. Remarkably, we find that excitations in an undirected graph may travel across a link preferentially in one direction, despite the stochastic nature of the dynamics. Our results pave the way for advances in network controllability, performance tuning, and failure prediction.

Author contributions: P.M. and M.-T.H. designed research, performed research, analyzed data, and wrote the paper.

The authors declare no competing interest.

This article is a PNAS Direct Submission.

Data deposition: The code used to perform the analyses presented in the current study and the produced data are available in the public repository FigShare (https://figshare.com/projects/Asymmetry/79461).

[1]To whom correspondence may be addressed. Email: Paolo.Moretti@fau.de.

This article contains supporting information online at https://www.pnas.org/lookup/suppl/doi:10.1073/pnas.1919785117/-/DCSupplemental.

First published July 20, 2020.

pattern-forming capabilities of networks. In particular, they emphasize that the degree heterogeneity of the network is responsible for important features of the emerging (Turing) patterns (33). In this way, due to their much-larger-degree heterogeneity, Barabási–Albert (BA) graphs can be expected to display stronger patterns than Erdős–Rényi (ER) graphs. The phenomenon of self-organized excitation waves around hubs was discovered by Müller-Linow et al. (34) using the same discrete model of excitable dynamics as used here. Such patterns have also been experimentally confirmed in neuronal cultures in vitro (35). There, the authors attribute the emergence of such periodic global bursts to the noise-focusing effect facilitated by topological features in the network (35). In large-scale simulations of mammalian thalamocortical systems, one can also observe propagating waves spontaneously emerging at different locations of the cortex (36). In astrocyte networks, the emergence of calcium waves has been discussed (37).

We note here that most modeling approaches for complex networks have been node-centric in nature, i.e., they measure properties of a network by considering nodes as their elemental constituents. For instance, centrality measures aim at building a node hierarchy in a network, ranking nodes according to their degrees, their path betweenness, or their weights in a spectral decomposition. Interestingly, link-based centrality measures have received very little attention instead. A notable exception is the definition of edge betweenness (38) and its recent application to failure prediction in network models of materials and structures under mechanical load (39, 40). Basic phenomena such as wave propagation, simple in Euclidean geometries, may need even more complex tools: The systematic advancement of a wave front implies the systematic usage of certain links, and systematically in one direction. Understanding how frequently a given link (ij) will host the passage of an excitation in each direction requires a new toolset, which allows one to quantify how central that link is (i.e., how close to the wave source), but also how prevalent the wave propagation will be in the $i \to j$ direction rather than in the $j \to i$ direction. This type of oriented link centrality should allow one to predict the prevalence of link usage in a given direction, providing fruitful information e.g., for performance-critical systems where link overload in a given direction may lead to disruption and failure, a type of information that current models and techniques still cannot provide.

We address this conceptual gap of a link-centric study of network dynamics by introducing a structural measure. This measure is based on oriented link centrality, the set-orientation prevalence of a link with respect to a set of hubs. Our study is motivated by the need to quantify wave patterns in networks, as one of the most prominent forms of self-organized dynamic patterns. In the simplest representation of such systems, nodes can be in a susceptible, excited, or refractory state. In Euclidean geometries, it is easy to visualize propagating fronts of each of those phases invading one another, in what we commonly identify as a *wave*. In complex networks, instead, we do not have a fixed spatial embedding of the networks, nor do we have a unique distance on it—in other words, we lack an embedding-independent way to visualize and measure waves. Our results show that our newly defined orientation prevalence of a link with respect to a set of source nodes correlates positively with the probability of a link to preferentially propagate activity in the direction *away* from that source set, within the standard shortest-path metric. Our results are independent of the choice of graph embedding—in fact, they do not require any. In passing, we are able to show essential differences in wave propagation within BA and ER graphs. For BA graphs, self-organized wave patterns have been discussed and linked to the graph's hubs as wave centers (34). Here, we show that ER graphs do produce waves, too, although generated by a much larger core.

The phenomenon that in excitable dynamics on graphs some links are systematically used in a unidirectional fashion has not been explored in detail. Understanding how such asymmetric link usage depends on the network architecture and on the parameters of the dynamic can be expected to provide fundamental insight into the relationship of network topology and dynamics.

Methods

Dynamical Model and Link-Usage Asymmetry. In the following, a three-state stochastic cellular automaton is used as a stylized model of excitable dynamics. The model operates on a state space of susceptible (S), excited (E), and refractory (R) elements. Transitions are $S \to E$ if an excitation is in the direct neighborhood of the node in state S (i.e., the activation probability is one in our model), $E \to R$ (i.e., the duration of an excitation is one time step); with the (recovery) probability p, $R \to S$, leading to a geometric distribution of refractory periods around an average refractory time of $1/p$; with the (spontaneous activation) probability f, $S \to E$, even when there is no excitation in the neighborhood. This model (or variants thereof) has been studied in a range of investigations (34, 41–45).

Simulation runs of this model can then be used to compute the following quantities. Let $x_i(t) \in \{S, E, R\}$ be the state of node i at time t for SER (susceptible–excited–refractory) dynamics on a network $G = (\mathcal{V}, \mathcal{E})$ with a node set $\mathcal{V}$ and a link set $\mathcal{E}$. The network can also be represented via its adjacency matrix A_{ij}. It is convenient to discuss the excitation pattern instead:

$$c_i(t) = \begin{cases} 1, & x_i(t) = E \\ 0, & x_i(t) = S \vee R. \end{cases}$$

In this way, we can define a sequential activation (or signal propagation) matrix,

$$C_{ij}^{(+)} = C_{i \to j} = \sum_t c_i(t) c_j(t+1),$$

(see also refs. 6 and 43 for details on these quantities). In some cases, it is more convenient to consider normalized version of this matrix. Let

$$c_i^* = \sum_t c_i(t),$$

denote the total number of excitations of node i in the time series under consideration. Then, the normalized quantities $\sigma_{i \to j}$ of the signal propagation matrix are defined as $\sigma_{i \to j} = C_{i \to j} / \min(c_i^*, c_j^*)$. Quantities in this matrix are normalized such that each entry is between zero and one. As the dynamics prohibit the excitation of the same node across multiple time steps, the diagonal elements of this matrix are zero, $\sigma_{i \to j} = 0$.

The link-usage asymmetry $\alpha_{(ij)}$ is the difference of the entries in the sequential activation matrix for the "forward direction" $(i \to j)$ and the "backward direction" $(j \to i)$ of a link (ij), i.e., $\alpha_{(ij)} = (\sigma_{i \to j} - \sigma_{j \to i}) / (\sigma_{i \to j} + \sigma_{j \to i})$. The vector $\alpha_{(ij)}$ is thus a vector with respect to the link set $\mathcal{E}$. Values for pairs of nodes that are *not* a link of the graph are not considered, as such elements are second-order effects generated by the asymmetries along the links of the graph.

A high positive value of $\alpha_{(ij)}$ thus means that excitations are traveling preferentially from node i to node j. A high negative value $\alpha_{(ij)}$ means that excitations are traveling preferentially from j to i, and a value of $\alpha_{(ij)}$ close to zero indicates no directional preference, as the contributions of both directions essentially cancel out.

In *Results*, we analyze simulations for networks of sizes $N = 10^3$ and $N = 10^4$, unless otherwise specified. Each simulation set includes multiple realizations of a given network model (BA or ER graph, of a fixed size and a given average degree $\langle k \rangle$). For each network realization, the SER dynamics simulation is repeated for multiple random choices of initial states. Initial states are assigned as described in ref. 43, as fixed fractions of susceptible, excited, and refractory nodes. Each simulation set allows us to compute a set of values $\alpha_{(ij)}$, each one representing the link-usage asymmetry of an individual link of a given network, averaged across the multiple runs of the dynamics (multiple initial conditions).

Graph Models and Topological Properties. As network models, we use standard random (ER) and preferential attachment (BA) graphs. In both cases, the two parameters are the network size N and the average degree $\langle k \rangle$. All links are labeled according to $i > j$, while nodes $i = 1, 2, \ldots, N$ are labeled such that $k_i \geq k_j$. In this way, all degree gradients are nonnegative, $g = k_i - k_j \geq 0$. Note that our results do not depend on this choice of

labeling (see below). All results have also been verified by using a random labeling of nodes and links.

The quantity $\pi_{(ij)}(H)$ measures the orientation "prevalence" of a link with respect to a set of hubs $H \subset \mathcal{V}$. The *hub-set-orientation prevalence* counts the number of times a link is perceived as pointing "outward" from a given hub $h \in H$ minus the number of times the link is perceived as pointing "inward" to the hub. The formal definition of "pointing outward and inward" is the following: Given a link $(ij) \in \mathcal{E}; i, j \in \mathcal{V}$ in the graph $G = G(\mathcal{V}, \mathcal{E})$ and one node $h \in H \subset \mathcal{V}$ out of the set of hubs H, we compute the shortest-path distance from the hub h to the nodes i and j defining the link, d_{hi}, d_{hj}. If $d_{hi} > d_{hj}$, the link is considered pointing inward; if $d_{hi} < d_{hj}$, the link is considered pointing outward; cases where $d_{hi} = d_{hj}$ are neutral with respect to this prevalence count; in this case, the link is oriented tangentially with respect to the hub h. More formally, the orientation of a link $(ij) \in \mathcal{E}$, $i, j \in \mathcal{V}$ with respect to the node $h \in \mathcal{V}$ is given by

$$\omega((ij), h) = \Theta\left(d(i, h) - d(j, h)\right) \quad [1]$$

with $\Theta(x)$ as the usual step function,

$$\Theta(x) = \begin{cases} 1, & x > 0 \\ 0, & x = 0 \\ -1, & x < 0 \end{cases}. \quad [2]$$

The hub-set-orientation prevalence of the link (ij) is then

$$\pi_{(ij)}(H) = \sum_{h \in H} \omega((ij), h). \quad [3]$$

As in the case with the asymmetry, the prevalence is only evaluated for links of the graph, i.e., $A_{ij} = 0 \Rightarrow \pi_{(ij)} = 0$. Note that we are assuming a certain order of representing the (undirected) links of the graph in terms of pairs of nodes. Considering the previous example of the link (ij) in the graph, this means that (ij) is present in the list of links and, formally, (ji) is not. In particular, the sign of $\pi_{(ij)}(H)$ depends on the ordering of the two nodes forming the link, $\pi_{(ij)}(H) = -\pi_{(ji)}(H)$. This arbitrary assignment of ordering of nodes in the pair representing a link has no effect on the results presented here, as it is done consistently for the dynamical assessment of a link (via the link-usage asymmetry $\alpha_{(ij)}$) and the topological assessment (via the degree gradient $k_i - k_j$ and the prevalence $\pi_{(ij)}$).

As for the link-usage asymmetry, each simulation set includes multiple realizations of a given network model (the same as those used to compute link-usage asymmetry). For each network realization and for each choice of the hub-set size, a single value of the hub-set-orientation prevalence is associated with every link of such network. This allows us to construct a set of values of $\pi_{(ij)}$ in a one-to-one correspondence with the values of $\alpha_{(ij)}$ discussed above.

Pattern Predictability. We show in *Results* that the hub-set-orientation prevalence introduced above correlates positively with asymmetric link usage. To quantify this correlation, we define the "pattern predictability" as the Pearson correlation coefficient between link-usage asymmetry and hub-set-orientation prevalence. We recall here that for each simulation set, and for each choice of the hub set, we compute a set of link asymmetries and a corresponding set of hub-set-orientation prevalence values, one for each link. Across network realizations, we identify classes of links characterized by the same degree-gradient value. For all links belonging to the same degree-gradient class g, and for a given hub set H, we compute the Pearson correlation coefficient ρ_g between the values of $\alpha_{(ij)}$ and $\pi_{(ij)}(H)$ with $i, j \in \mathcal{V}$, $(ij) \in \mathcal{E}$, and $k_i - k_j = g$. The pattern predictability is then defined as the average of ρ_g across degree-gradient classes. Pattern predictability thus measures how strong the correlation is between the emergence wave-like excitation patterns and the topological orientation of links with respect to a restricted set of hub sources. It is by definition embedding-independent, as it relies solely on the intrinsic shortest-path metric, through the hub-set-orientation prevalence.

Pattern Strength. The pattern-predictability measure defined above allows us to generalize the concept of waves to the intrinsic metric of a complex network, in an embedding-agnostic fashion. The question remains, whether such waves can actually be detected in the more traditional sense, i.e., as emanating wave fronts in the Euclidean space, in which the graph is embedded and the functional activity patterns develop. In order to address this question, we introduce an embedding-dependent measure of wave-signal strength, which we call "pattern strength." Given a real networked system and its spatial embedding $\mathcal{S}$, $\mathcal{S}$ defines a $d-$dimensional Euclidean space, in which we choose a frame of reference where the origin coincides with the network center of mass. In polar/spherical coordinates, r identifies the radial coordinate measured from the center. Starting from simulations for an individual network realization (single network, multiple realizations of the dynamics and variation of the initial state), we can identify the m_r nodes and $n_r = m_r(m_r - 1)/2$ node pairs in the shell of radial coordinate r for a certain bin size Δr. The pattern strength at r, $z(r)$, is thus defined as the difference between the average simultaneous coactivation probability for the n_r pairs at r and the same probability for a random choice of n_r pairs across the network, normalized by the SD of the probability in the set of random choices. This definition is equivalent to a statistical z-score, in that it quantifies simultaneous coactivation in terms of its deviation from the average behavior (or null hypothesis). Positive values of $z(r)$ thus indicate a node shell which exhibits higher-than-average coactivation, which we identify as the signature of systematic wave propagation. This definition of pattern strength requires a spatial embedding of the graph. We here use a refined version of the standard spring embedding algorithm. Details of our approach are given in *SI Appendix*.

Data Availability.

The code used to perform the analyses presented in the current study and the produced data are available in the public repository https://figshare.com/projects/Asymmetry/79461.

Results

Illustration of Hub-Set-Orientation Prevalence. We start with the main topological quantity of our investigation, the hub-set-orientation prevalence. The set-orientation prevalence of a link with respect to a set H of hubs quantifies the typical (or average) orientation of the link (which node of the link is encountered first?), when passing from each hub in the hub set to the two nodes forming the link (*Methods*). Fig. 1 illustrates the concept of a hub-set-orientation prevalence for a small random graph (Fig. 1*A*) and for two 200-node representatives of BA and ER graphs, respectively (Fig. 1*B*). In the example in Fig. 1*A*, only two links have the same orientation with respect to all $|H| = 4$ hubs and, hence, have maximal prevalence. These are shown in red in Fig. 1*A*. Already on this illustrative level, a strong topological difference between BA graphs (Fig. 1 *B*, *Left*) and ER graphs (Fig. 1 *B*, *Right*) becomes apparent: In BA graphs, even for intermediate hub-set sizes, typically many more links have maximal orientation prevalence than for ER graphs.

On the level of the dynamics, the main quantity of interest is the link-usage asymmetry. The predictive power of the hub-set-orientation prevalence for this link-usage asymmetry is the focus of our subsequent investigation.

Link-Usage Asymmetry in BA and ER Graphs. The main result of our investigation, the systematically strong pattern predictability—as quantified by the correlation between hub-set-orientation prevalence and link-usage asymmetry—is shown in Fig. 2 for different networks and parameters of the dynamics. Fig. 2*A* shows the correlation between asymmetry and prevalence in a BA graph of 1,000 nodes. The corresponding figure for an ER graph is given in *SI Appendix*, Fig. S3. As a real-world application, Fig. 2 also contains results for the human connectome from refs. 17 and 46. We will discuss these results in detail below.

In order to assess the visual impression from Fig. 2*A* on a more quantitative level, we compute the pattern-predictability individually for each value of the degree gradient (*Methods*). For BA graphs, this is depicted in Fig. 2*B* for different values of the rate of spontaneous activity, f. Similar results hold for ER graphs. *SI Appendix*, Fig. S4 shows typical scatter plots of link-usage asymmetry vs. hub-set-orientation prevalence for individual degree-gradient classes.

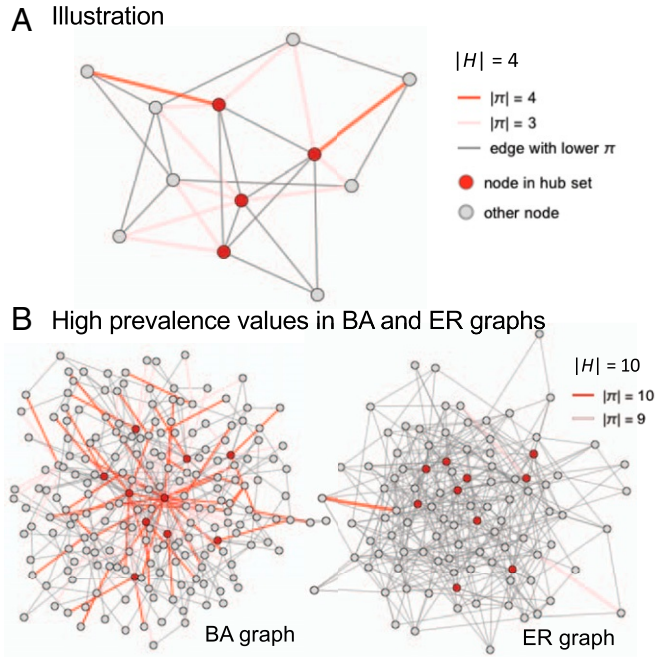

Fig. 1. Illustration of the hub-set-orientation prevalence. (*A*) For a small random graph ($N = 12$ nodes, $M = 30$ links) and a hub-set size of $|H| = 4$ (with the hub set H consisting of the $|H|$ highest-degree nodes; shown in red), the orientation prevalence $\pi_{(ij)}(H)$ of each link (ij) is computed. Links with maximal orientation prevalence $|\pi_{(ij)}(H)| = |H| = 4$ are shown in red, and links with an orientation prevalence of $|H| - 1$ are shown in light red. (*B*) Examples of graphs (*Left*, BA; *Right*, ER), for which the links with maximal (red) or near-maximal (light red) orientation prevalence for an intermediate-size hub set ($|H| = 10$; hub-set nodes shown in red) are highlighted.

Here, a purely topological quantity, the hub-set-orientation prevalence, correlates with a quantity derived from the dynamical excitation patterns, the link-usage asymmetry, even when we account for the local topological contributions to this asymmetry by looking at the pattern predictability for each degree gradient individually. *SI Appendix*, Movie S1 illustrates our findings using a small BA graph as an example. In this movie, link-usage asymmetry is depicted in a cumulative fashion, which highlights that the stable asymmetry pattern emerges from the iterative action of consecutive waves. In addition to f, three other parameters affect this result: the hub-set size $|H|$, the recovery probability p, and the average node degree $\langle k \rangle$. Dependence of pattern-predictability values for different degree-gradient classes on these parameters are summarized in *SI Appendix*, Figs. S5 and S6.

In Fig. 2*B*, one finds high positive correlations across the whole range of degree gradients. Only at degree gradients close to zero do the correlations depend systematically on the rate of spontaneous activity f with increasing f reducing pattern predictability. For other regimes of the degree gradients, the predictability is essentially independent of f, provided $f \neq 1$. At high degree gradients, fluctuations increase due to the rare occurrence of these cases. As already pointed out in earlier work (43, 45), the discrete nature, in space, time, and state space, of our minimal model of excitable dynamics is instrumental in defining the key quantities investigated here, namely, the notion of sequential activation (as opposed to, e.g., coactivation) and, hence, the quantitative assessment of link-usage asymmetry.

An important parameter of our analysis is the size of the hub set. In order to understand how this parameter affects pattern predictability, Fig. 2*C* shows the pattern predictability (averaged over all degree gradients) as a function of the hub-set size. For both graph types, the curves are increasing with increasing hub-set size, suggesting that the orientation prevalence established by a small initial set of highest-degree nodes (even in the case of ER graph, where the degree is more uniform) is not altered, but strengthened with increasing hub-set size. The two most prominent differences between BA and ER graphs in Fig. 2*C* are 1) the steeper increase of the BA curve (fewer hubs already lead to a prevalence capable of explaining the numerically observed link-usage asymmetry, suggesting that individual hubs and small, "rich-club"-type groups of hubs serve as organizers of the global patterns); and 2) the higher values of the average correlation for ER graphs, compared to BA graphs, for large hub sets (suggesting that the global patterns are organized around a large group of nodes, a "core" of the graph, and not around individual nodes or rich clubs).

The rapid increase of this curve for the BA graphs in comparison to the much broader curve in the case of ER graphs in Fig. 2*C* also suggests an interesting feature of the hub-set-orientation prevalence on purely topological grounds: For BA graphs, the information about the prevalence of the link is distributed among few hubs. Increasing the hub set beyond these few nodes essentially reiterates information already provided by these few hubs, as shortest paths toward the link under consideration will traverse one of these hubs. In the case of ER graphs, additional nodes entering the hub set still can contribute new information about the prevalence of a link.

Link-Usage Asymmetry in the Human Connectome. In order to see whether our findings of self-organized, global excitation patterns, together with their explanation via the hub-set-orientation prevalence, can also be found beyond generic models of random graphs in realistic architectures of biological neural networks, we simulated activity patterns on the human connectome from refs. 17 and 46. This 998-node network is known to have a pronounced rich-club organization (27). At the same time, partly due to its obvious spatial embedding, it has a strong modular structure (47, 48). Fig. 2 *D* and *E* show the various aspects of pattern predictability discussed before—the scatter plot of link-usage asymmetry and hub-set prevalence, the correlation of these two quantities for different degree gradients, and the average pattern predictability as a function of the hub-set size—for this connectome architecture. Due to the higher connectivity of this graph, we reduce the value of the recovery probability p for better comparability to our previous results for BA and ER graphs. It is quite striking that the same set of phenomena is observed for the connectome architecture, confirming that, here as well, the rich-club structure serves as an organizer of collective excitation patterns. It is also seen, though, that the initial increase of pattern predictability with the hub-set size is much slower than for a BA graph and resembles more that for an ER graph with its more distributed core. This is due to the fact that the hubs in the human connectome are distributed across modules, thus effectively broadening the core: With increasing hub-set size, new hubs joining the set continue to contribute new information about the orientation prevalence of links, in contrast to the BA graph, where, quite rapidly, the information contributed by additional hubs becomes redundant, as shortest paths toward individual links are the same as for previous hubs.

Impact of Rich-Club Organization. The functional role of a rich-club organization is under vivid debate in neuroscience (see, e.g., refs. 31, 49, and 50). We hypothesize that pattern predictability (i.e., the explanation of link-usage asymmetry by the hub-set prevalence) is greatly influenced by the rich-club organization of a graph. In order to quantitatively test this hypothesis, we start from the standard BA graph, which already has a pronounced

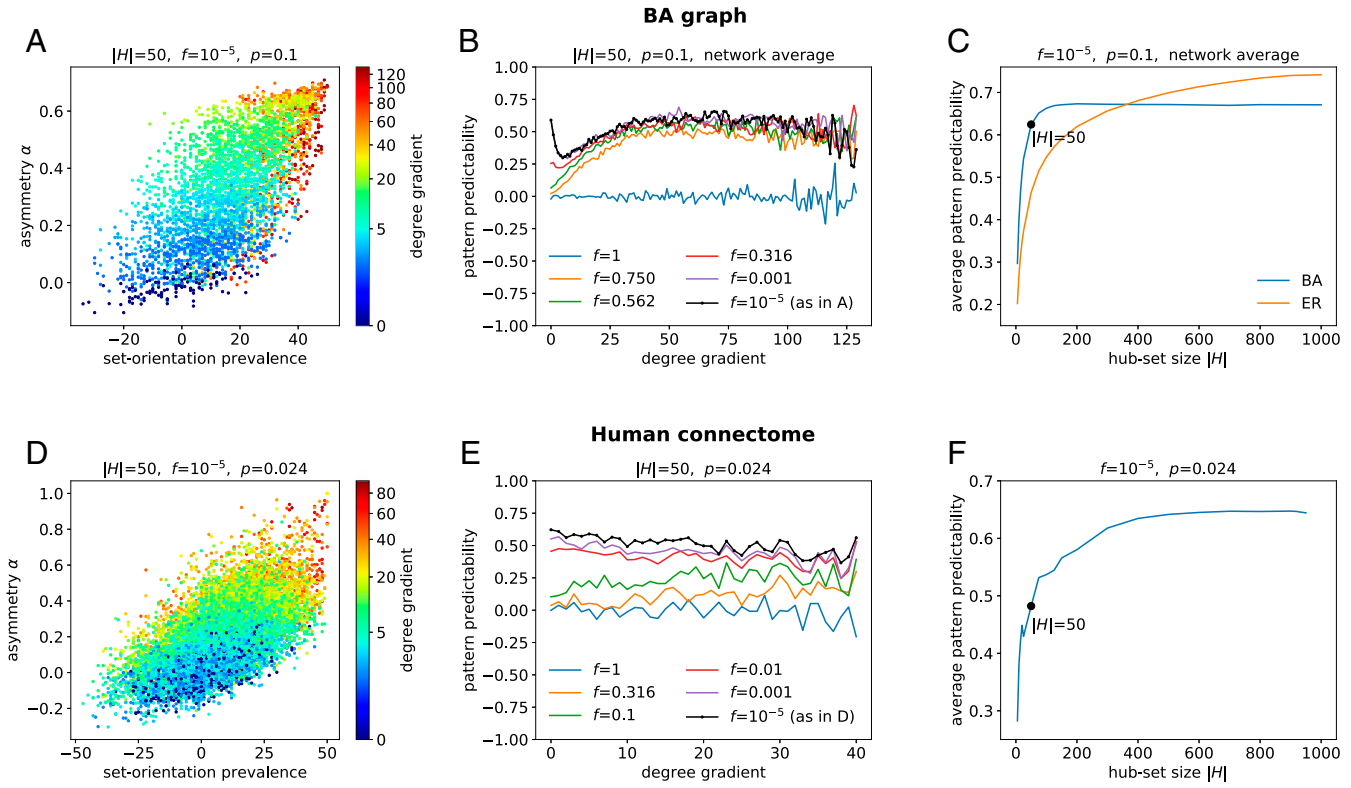

Fig. 2. Link-usage asymmetry and pattern predictability. (*A*) Link-usage asymmetry in a BA graph correlates to both degree gradients and set-orientation prevalence. Each point corresponds to a link in the network. Different colors indicate different degree gradients of each link. Asymmetry in link usage correlated positively to both degree gradients (local patterns) and set-orientation prevalence (self-organized, nonlocal patterns). Set-orientation prevalence is computed for link (*ij*), with respect to the forward direction $i \to j$ for a hub-set size $|H| = 50$. As discussed in *Methods*, all links are labeled according to $i > j$, while nodes $i = 1, 2, \ldots, N$ are labeled such that $k_i \geq k_j$. Upon using a random node-labeling scheme, the cloud plot becomes symmetric around the origin, and degree gradients appear with both signs. The positive correlations, however, remain qualitatively unaffected. In this figure, a BA graph of N = 1,000 and $\langle k \rangle = 8$ was considered. Link-usage asymmetry was evaluated for SER dynamics, with $f = 1 \times 10^{-5}$ and $p = 0.1$, which ensures nonvanishing sustained activity. Data are collected from 100 realizations of the SER dynamics, each consisting of 2,000 time steps. (*B*) Pattern predictability for individual degree-gradient classes is computed as Pearson correlation coefficients, which are averaged over 100 realizations of networks as in *A* and shown here as a function of the degree gradient. Hub-set-orientation prevalence was computed for hub-set size $|H| = 50$. Link-usage asymmetry was evaluated for SER dynamics, with varying f and fixed $p = 0.1$. The presence of positive correlation at intermediate values of the degree gradients signals the emergence of nontrivial self-organized dynamic patterns. The case of $f = 10^{-5}$ (black curve) is the one examined further in the following. Similar results are obtained for any f other than $f \approx 1$. (*C*) Influence of the hub-set size and evidence of a well-defined source core. The average pattern predictability is plotted against varying choices of the hub-set size (for size one to the whole network size), for ER and BA graphs of N = 1,000 and $\langle k \rangle = 8$. Averages are taken over all degree-gradient classes and over 100 network realizations. While increasing the hub-set size, BA graphs rapidly settle to a nearly stationary value, indicating that the true core, from which dynamic patterns originate, is very limited in size, in agreement with our general understanding of scale-free network topology. ER graphs, on the other hand, exhibit a much slower increase, suggesting that the equivalent concept of a core in ER graphs is significantly larger and less localized. (*D–F*) Same as *A–C*, respectively, in the case of the human connectome structural network ($N = 998$). Note that the average pattern predictability (*F*) has an initial quick increase, akin to that of the BA case (*C*), as a result of a *strong* hub set. The subsequent slowdown, instead, is due to the less centralized, modular structure of the connectome.

rich-club structure, and systematically decrease and increase the strength ϕ of the rich-club organization. Given a certain rich-club size $|R|$, we count the number of links among these $|R|$ highest-degree nodes forming the set R and denote this situation as $\phi = 1$. Randomly removing 10% of these links leads to $\phi = 0.9$, while randomly adding the same amount of links among the $|R|$ nodes yields $\phi = 1.1$, and so on.

Fig. 3 shows the pattern predictability as a function of the hub-set size for BA graphs manipulated in this way for different values of the rich-club strength ϕ. The curve for $\phi = 1$ is the same as in Fig. 2*C*. We see that the sharp increase of pattern predictability at small hub-set sizes is not strongly affected. However, the asymptotic behavior of pattern predictability at large hub-set sizes varies systematically with ϕ. This shows that, indeed, with increasing rich-club strength, link-usage asymmetry aligns more and more strongly with the topological layout measured by the hub-set-orientation prevalence.

Further Interpretation of Pattern Predictability. Pattern predictability compares two quantities: 1) the link-usage asymmetry obtained from numerical simulation of excitable dynamics on the graph and 2) the hub-set-orientation prevalence obtained just from the topology of the graph. Pattern predictability thus measures the association of a property of the excitation pattern with the property of network architecture. Both quantities evaluated on each link of the network do not depend on the embedding of the graph in a reference space.

Regarding our terminology, a set-orientation prevalence can be defined for any set of nodes, and we believe that other definitions of node sets may lead to a useful quantity for diverse applications. Here, we compile node sets from the nodes with the highest degrees in the network. In the case of BA graphs and small set sizes, these are the hubs. In ER graphs, these will be the nodes with a slightly higher-than-average degree. With increasing set size, these "hub sets" get populated by ever more lower-degree nodes. We nevertheless call these sets "hub

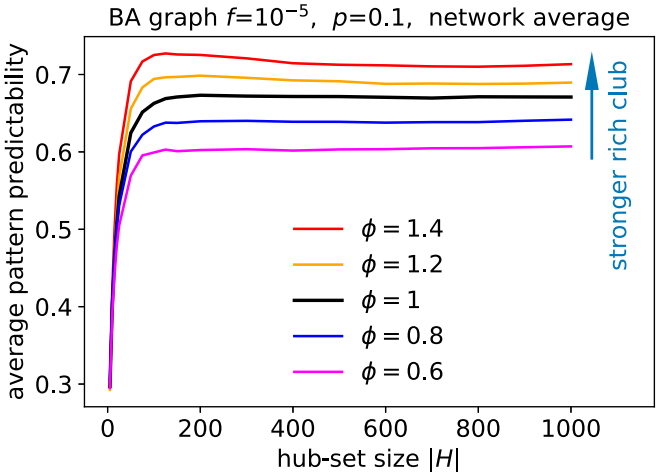

Fig. 3. Pattern predictability and rich-club strength. Average pattern predictability for BA graphs, as a function of the rich-club strength ϕ, is shown. We define the rich-club R as the set of the $|R|$ highest degree nodes in a graph. The $\phi = 1$ curve is for the reference set of BA graphs, the same as in Fig. 2C. The $\phi < 1$ curves are for the same set, where a fraction $1 - \phi$ of links connecting pairs of rich-club nodes is removed. The $\phi > 1$ curves are for the same set, where a fraction $\phi - 1$ of links connecting pairs of rich-club nodes is added. Here, we set $|R| = 100$. Qualitatively similar results are obtained for different choices of $|R|$.

sets" and use the term "hub-set-orientation prevalence" to indicate that our node sets are constructed from the nodes with the highest degrees.

Here, the computation of the average of pattern predictability over all degree gradients (i.e., over all points of a curve in Fig. 2*B*) serves as a means of condensing the information content of Fig. 2*B*, in order to directly compare BA and ER graphs. We checked that the result does not change qualitatively, when, for example, computing an average weighted by the number of cases in each degree-gradient class or when looking at individual degree-gradient classes separately as a function of the hub-set size.

At this level of consideration, the main difference between BA graphs and ER graphs is that for BA graphs, the pattern predictability (averaged over degree-gradient classes) as a function of the size of the hub set saturates much more rapidly at much smaller hub-set sizes, compared to ER graphs (Fig. 2*C*). Following our hypothesis that this contribution to the link-usage asymmetry is associated with waves of excitations establishing themselves in the graph in a self-organized fashion, this difference between BA and ER graphs suggests that 1) self-organized waves also emerge in ER graphs (as evidenced by the very-high-prevalence asymmetry correlation coefficients) and 2) a much larger set of nodes serves as the center of the self-organized waves (as evidenced by the saturation of the correlation coefficient at much larger hub-set sizes).

Relationship between Link-Usage Asymmetry and Collective, Self-Organized Excitation Patterns. We hypothesize that the observed link-usage asymmetry is a consequence of self-organized waves on the graph. On this basis, we provide numerical evidence that the hub-set-orientation prevalence, together with the local degree gradient, explains the main features of link-usage asymmetry. Waves can, from our perspective, only be meaningfully defined (and quantitatively assessed) with respect to a spatial embedding of the graph. Here, we introduce a direct measure of the self-organized patterns, via the coactivation statistics of nodes in the same radial distance from the network core, the pattern strength (*Methods*). If waves can be measured in a spatial embedding of some relevance to the system under consideration, are those wave patterns the same ones that we measure via the pattern of link-usage asymmetries in our embedding-independent approach?

In order to address this question, we define the pattern strength at distance r from the graph center of mass as the statistical z-score $z(r)$ of simultaneously active node pairs, averaged across multiple realizations of our SER dynamics (*Methods*). Distance and center of mass are defined starting from the natural embedding of the graph at hand. Since in our study we deal with synthetic networks, we choose the natural embedding based on information-theory considerations: In the absence of further constraints, the most probable configuration will obey a maximum-entropy principle. Our method is detailed in *Methods* and is reminiscent of the approach proposed by Müller-Linow et al. (34), who showed that clusters of coactivating elements strongly overlap on the topological side with "topological shells," i.e., sets of nodes with the same distance from a dominant hub. Fig. 4 shows pattern strength for BA and ER graphs of equal sizes and average degrees.

Positive values of the pattern strength $z(r)$ in the radial shell at distance r from the center of mass indicate that the coactivation at r is higher than the one obtained from a reference random sampling (null model) of the same size. Conversely, negative values of $z(r)$ for large r trivially indicate lower-than-average coactivation rates: If sets of nodes at small radii show systematically elevated coactivation and, hence, lead to high z scores, sets of nodes at large radii will necessarily yield negative z scores, as the collective of all nodes serves as the null model. The nonuniform, decreasing radial dependence of the pattern strength points to a persistent breaking of spatial symmetry, highlighting a preferential radial arrangement for coactive node pairs, which we identify as a wave, in line with the previous investigation for BA graphs (34). In passing, we note that, indeed, self-organized waves exist in ER graphs as well, according to the data in Fig. 4. This result confirms the observation of a larger core in ER graphs, as the maximum pattern strength is reached at larger radial distances.

Our analysis points to a tight coupling between the large-scale, collective patterns, as measured by the pattern predictability, and the self-organized excitation waves, quantified by the pattern strength. It is in particular evident that both routes point to the existence of a core, a set of source nodes from which waves propagate. Our results show that the concept of core emerges from the intrinsic network metric and is confirmed by the extrinsic Euclidean metric induced by a standard embedding algorithm, without any fine tuning. While this result is already remarkable in its own right, we may wonder to which extent we can further push this analogy. Do both methods identify the same cores? Do they point to the same waves?

Fig. 4 shows that in BA graphs, the answer to these questions is indeed affirmative. Across a population of 32 networks, we monitor the correlation between our two indicators, 1) pattern strength, for the inner shell in the spatial embedding (the 10 innermost nodes); and 2) pattern predictability, for increasing sizes of the hub set. Pattern predictability (correlation between asymmetry and orientation prevalence) and pattern strength (nonrandom coactivation of radial node sets) will vary from network realization to network realization. The positive correlation in Fig. 4 indicates that in network realizations with a high pattern predictability, also the pattern strength is high, and vice versa. Not only is this correlation measure positive for small-to-moderate set sizes, it actually peaks at values of the set size that are comparable to the inner-shell size. Examples of the scatter plots underlying these correlations are compiled in *SI Appendix*, Fig. S8. It should be noted that the measurement of this covariation signal is highly nontrivial: The pattern predictability itself is a statistical quantity (a correlation coefficient averaged over

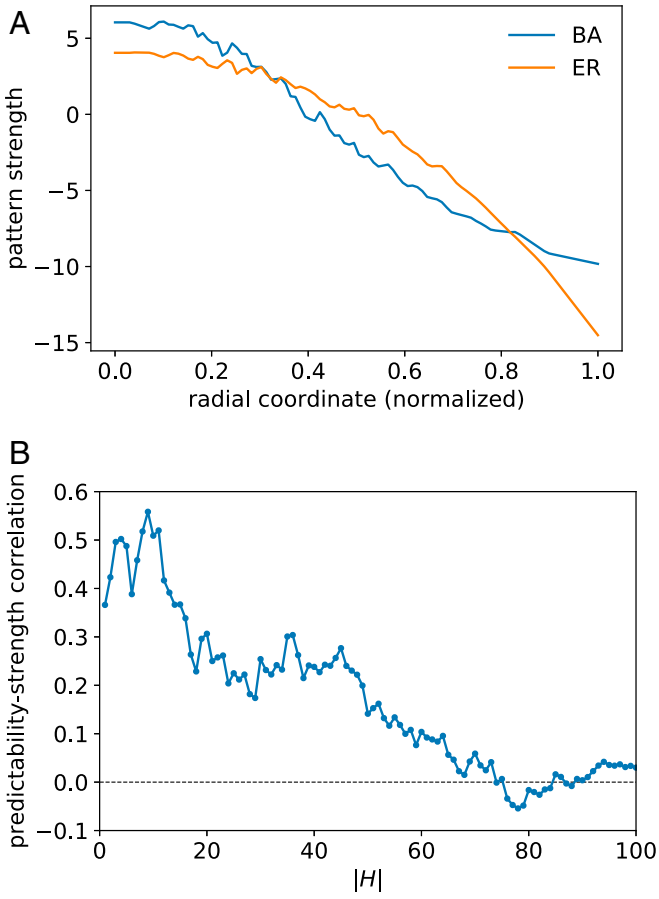

Fig. 4. Collective patterns in embedded graphs. (*A*) Evidence of wave patterns in embedded BA and ER graphs. We plot the pattern strength as a function of the radial coordinate in a BA and ER graph. Radial coordinates are computed for a spring-embedded BA graph of size $N = 10^4$, obtained by means of the maximum-entropy principle (*Methods*). Positive values along the vertical axis indicate a systematic presence of simultaneously active nodes at a given distance, the signature of a propagating wave front. Coactivation data are computed starting from SER simulations with $f = 1 \times 10^{-5}$ and $p = 0.1$. Bin size is varied across the curves, in such a way that all bins contain the same number of nodes. The procedure is repeated for multiple realizations of each network model (BA and ER), and the radial coordinates are each time normalized by the network radius. (*B*) Correlation of pattern predictability and pattern strength in BA graphs. We show here the Pearson correlation coefficient of values of pattern predictability and pattern strength, across multiple network realizations. Since the pattern predictability depends on the size of the hub set $|H|$, we plot the correlation coefficient as a function of $|H|$.

degree classes), and the pattern strengths at different radial shells are not independent, as discussed above.

The systematic emergence of positive correlations in this context thus confirms how strong the wave picture is in BA graphs and how clear-cut the concept of a core is in such graph models. While this is to be expected in graphs of this type, characterized by a dominant hub structure, a related question would be how this picture changes in graphs with less-centralized topological features. To answer this question, we have extended the same analysis to our set of ER graphs. Not surprisingly, a systematically positive curve such as the one in Fig. 4 cannot be obtained in this case (*SI Appendix*, Fig. S7). Correlation values are highly fluctuating and also depend erratically on the size of the inner shell. This is due to fluctuations of the size of the self-organized core serving as the center of the collective waves and provides tangible evidence of the fact that, while waves are still recorded in ER graphs, the core they originate from is broader, and the separation between core and noncore nodes is weaker.

Discussion

Our findings touch upon the functional role of rich clubs in complex networks (31, 49, 50) and the ongoing debate on the relationship between structural and functional connectivity in neuroscience (51–53). The application of our framework to the human connectome from refs. 17 and 46 shows that the phenomenon of link-usage asymmetry, together with its topological interpretation via orientation prevalence, not only holds for generic random graphs, but also for real biological connectivity patterns.

Our statements about self-organized patterns on graphs have been exemplified for the case of excitable dynamics. As illustrated by a range of investigations, wave phenomena (34, 36, 54), as well as spiral waves and other self-organized dynamical phenomena of excitations on graphs (43, 54–56), are contributing to the systematic relationship between network topology and dynamics (5, 57). Our investigation addresses the emergence of link-usage asymmetry in excitable dynamics on networks and, in particular, how self-organized collective excitation patterns contribute to this asymmetry.

The general concept of self-organized patterns, its potential relation in link-usage heterogeneities and asymmetries, as well as the new topological characterization of links via their orientation prevalence, however, go far beyond this main application domain. The emergence of asymmetries in the direction in which a link is used is far from trivial. In the paradigmatic example of a random walk, each link (ij) is taken by the walker in either direction with identical probabilities. This can be understood easily, considering that the probability of an $i \to j$ step is independent of i and j, as it is proportional to the occupation probability of i, which is proportional to the degree k_i, times the probability of choosing j as the next walker position, proportional to $1/k_i$. Recently, a variant of link-usage asymmetry has been studied within a random-walk paradigm (58). In other dynamic processes, more complex than a random walk, it can be mechanistically clear that the difference between the degrees of the two nodes forming the link under consideration, the degree gradient along the link, is proportional to the probability of using this link in a particular direction. This is certainly the case for the excitable dynamics discussed here (see also the corresponding analytical treatment in *SI Appendix*). Attributing asymmetry solely to degree gradients is, however, too simplistic when one's focus is on collective self-organized patterns. Degree gradients exclusively result in *local* asymmetry—that is, asymmetry in the dynamics limited to the link whose degree gradient is being evaluated. More complex *nonlocal* dynamic patterns, such as waves, are notoriously observed in lattice topologies, and, realistically, such patterns may carry over to complex networks. Unlike lattices, where, e.g., wave patterns may be easily quantified thanks to the natural geometric embedding of the graph and its metric structure, complex networks require the definition of novel observables in order to measure directional patterns of propagation, which go beyond the local nature of degree gradients. As shown in *Results*, within each degree gradient class, the numerically observed link-usage asymmetry correlates very strongly with another, more global topological quantity—the hub-set-orientation prevalence of the link. This quantity, which characterizes the orientation of the link with respect to a predefined set of hubs, thus provides a topological explanation for the other (mechanistically less obvious) component of the dynamical signal, the link-usage asymmetry.

Our minimal model of excitable dynamics has two parameters, the recovery probability, p, and the probability of spontaneous excitations, f. At high f, the dynamics become predominantly

noise-governed, the sequential activation matrix σ becomes more symmetric, and the cumulative asymmetry (sum of all asymmetry values over all links) approaches zero. Changes of the recovery probability p lead mostly to a temporal rescaling with low p "slowing down" the dynamics, such that longer time series are required to accumulate a statistically sufficient amount of sequential activation data. Most importantly, the link-usage asymmetries remain robust over a wide range of parameter choices (p, f): Except for the effect of small fluctuations, the curves in Fig. 2*B* tend not to cross and are slowly changing over a broad range of parameter values.

We stress here that our approach to the characterization of dynamics in networks focuses on the measurement of spatiotemporal patterns. This is somewhat different from the statistical physics perspective, which often centers around system-wide critical phenomena, such as spontaneous symmetry breaking and continuous phase transitions. While the latter approach has been crucial to fully understanding complex phenomena such as the emergence and vanishing of epidemic thresholds, phase coherence, and percolation transitions (7, 59, 60), we believe that current advances in experimental data acquisition have exposed us to a level of detail that is usually averaged upon by standard coarse-graining techniques. Such detail seems to be crucial, e.g., to the inner workings of brain networks: While it is widely accepted that globally, the brain works in a critical-like state (60, 61), an increasing number of studies have recently focused on the mesoscopic dynamics, which shows traits of localization (24, 62, 63), coexistence, and pattern formation (6, 21, 42). Such patterns are nonlocal in nature, yet not global, as those normally take into account in models of continuous phase transitions. Even in the case of epidemic threshold studies in scale-free networks, such nonlocal patterns as the hub-reinfection mechanism have been proposed, in order to explain anomalies in the value of the threshold (7, 64). We note that this mechanism is, in essence, a consequence of the wave emanation that we study here.

We also reiterate that our approach is centered around links and activation, rather than node and activity. While this distinction may seem academic at first, it is much less so in the case of biological networks, which, unlike many techno-social networks, exhibit a hierarchy of links rather than (or on top of) a hierarchy of nodes. Biological networks are modular and hierarchical modular in nature, which means that different types of links ensue, depending on whether they are intramodular or intermodular and, in the latter case, to which hierarchical level they belong (see also the distinction between "dependency links" and "connectivity links" in interdependent networks in refs. 65 and 66). Inevitably, links belonging to different classes will naturally exhibit different set-orientation prevalence values and host different nonlocal dynamics patterns. In a complex system as the brain, the addition of our link-centric perspective is, in our opinion, essential, in order to complement the more traditional node-centered approach.

Conclusion

We have introduced a methodology to address the study of nonlocal activity patterns in graphs hosting excitable dynamics. Complex networks are characterized by localized topological features such as hubs or modules, small groups of nodes with prominent roles in excitable dynamics, which may promote wave patterns and sustained reactivation. These dynamic patterns are themselves localized in nature, as they occur on length scales much shorter than the correlation lengths emerging in critical phenomena. Our methods allow for the identification of those self-organized nonlocal patterns by the *small* sets of nodes acting as sources and the large set of links relaying activity in a preferential direction. Recent advances in neuroimaging and network-modeling techniques have shown that brain function may rely on a broad catalog of analogous self-organized nonlocal patterns, promoted by certain localized regions, often dubbed rich club, as well as by densely connected modules. Beyond the classical notion of a rich club, where a cluster of hubs interconnects the network communities, we see here the role of a rich club as a "network core" facilitating the emergence of complex patterns. While these self-organized patterns are normally coarse-grained over by standard statistical methods, they may prove just as important to the normal brain function as the global fluctuations of scalar-order parameters. This may especially be the case in pathological situations, in which the criticality hypothesis cannot be invoked, such as traumatic brain injury or Alzheimer's disease (29, 30, 32).

In our study, we used excitable dynamics as the paradigmatic process leading to pattern formation. These dynamics are relevant to various other fields of applications beyond neuroscience. Similar models to the SER model discussed here have been successfully employed for the study of epidemic thresholds (64), the effect of long-distance flight networks on disease propagation (67, 68), and the impact of population distributions and recurrent mobility patterns on the spread of epidemic diseases (5). The link-usage asymmetry studied here can, for example, guide vaccination schemes beyond the established hub-based immunization strategy (69, 70). Similar rules, as for the propagation of epidemic diseases, underlie the spread of information in a network (71). Realistic modeling of a specific system would, of course, require finer and more complex multiparameter models. The choice of such a purposely simple model is, however, necessary, if our aim is that of highlighting a connection between link-usage asymmetry and our newly introduced set-orientation prevalence as a fundamental property, and not as the result of parameter fine-tuning. Our stylized dynamics serves as a stepping stone in establishing fundamental relationships between network topology and dynamics, rather than in parameterizing a system-specific numerical model.

We expect that further details about the asymmetry may depend on the exact model of excitable dynamics. In the model discussed here, a single excitation is enough to trigger a subsequent excitation. Either absolute thresholds (like discussed in other works; ref. 61) or relative thresholds (a certain percentage of neighbors needs to be active to trigger an excitation; ref. 25) can also be explored. It seems intuitive, for example, that in relative threshold models, the contribution from the degree gradient will be less important.

Beyond the realm of neuroscience, our toolset appears relevant to networked techno-social systems exhibiting forms of eigenvector localization (72). Scale-free graphs of this type, like the BA graphs analyzed here, exhibit localization at their cores, identified by the highest-degree nodes or by the highest-ranking nodes in the so called k-core decomposition (73). As our hub-set-orientation prevalence relies on the accurate identification of a core, the possibility of interfacing our toolset to spectral methods thus appears extremely promising in further characterizing asymmetric propagation patterns.

ACKNOWLEDGMENTS. We thank Olaf Sporns for kindly giving us access to the human connectome data. P.M. was supported by Deutsche Forschungsgemeinschaft (DFG) Grants MO 3049/1-1 and MO 3049/3-1. M.-T.H. was supported by DFG Grant HU 937/7-1.

1. S. Boccaletti, V. Latora, Y. Moreno, M. Chavez, D. U. Hwang, Complex networks: Structure and dynamics. *Phys. Rep.* **424**, 175–308 (2006).
2. A. Arenas, A. Díaz-Guilera, J. Kurths, Y. Moreno, C. Zhou, Synchronization in complex networks. *Phys. Rep.* **469**, 93–153 (2008).
3. F. A. Rodrigues, T. K. D. Peron, P. Ji, J. Kurths, The Kuramoto model in complex networks. *Phys. Rep.* **610**, 1–98 (2016).
4. G. Yan *et al.*, Spectrum of controlling and observing complex networks. *Nat. Phys.* **11**, 779–786 (2015).

5. J. Gómez-Gardeñes, D. Soriano-Paños, A. Arenas, Critical regimes driven by recurrent mobility patterns of reaction–diffusion processes in networks. *Nat. Phys.* **14**, 391–395 (2018).
6. M. T. Hütt, M. Kaiser, C. C. Hilgetag, Network-guided pattern formation of neural dynamics. *Phil. Trans. R. Soc. B* **369**, 20130522 (2014).
7. R. Pastor-Satorras, C. Castellano, P. Van Mieghem, A. Vespignani, Epidemic processes in complex networks. *Rev. Mod. Phys.* **87**, 925 (2015).
8. W. Wang, M. Tang, H. E. Stanley, L. A. Braunstein, Unification of theoretical approaches for epidemic spreading on complex networks. *Rep. Prog. Phys.* **80**, 036603 (2017).
9. D. S. Bassett, O. Sporns, Network neuroscience. *Nat. Neurosci.* **20**, 353–364 (2017).
10. S. H. Strogatz, Exploring complex networks. *Nature* **410**, 268–276 (2001).
11. A. L. Barabási, *Network Science* (Cambridge University Press, Cambridge, UK, 2016).
12. M. Newman, *Networks* (Oxford University Press, Oxford, UK, 2018).
13. C. Song, S. Havlin, H. A. Makse, Origins of fractality in the growth of complex networks. *Nat. Phys.* **2**, 275–281 (2006).
14. M. Boguna, D. Krioukov, K. C. Claffy, Navigability of complex networks. *Nat. Phys.* **5**, 74–80 (2009).
15. A. L. Barabási, The network takeover. *Nat. Phys.* **8**, 14–16 (2011).
16. N. E. Radde, M. T. Hütt, The physics behind systems biology. *EPJ Nonlin. Biomed. Phys.* **4**, 7 (2016).
17. C. Honey *et al.*, Predicting human resting-state functional connectivity from structural connectivity. *Proc. Natl. Acad. Sci. U.S.A.* **106**, 2035–2040 (2009).
18. C. J. Honey, J. P. Thivierge, O. Sporns, Can structure predict function in the human brain?. *Neuroimage* **52**, 766–776 (2010).
19. A. M. Hermundstad *et al.*, Structural foundations of resting-state and task-based functional connectivity in the human brain. *Proc. Natl. Acad. Sci. U.S. A.* **110**, 6169–6174 (2013).
20. G. Deco *et al.*, Identification of optimal structural connectivity using functional connectivity and neural modeling. *J. Neurosci.* **34**, 7910–7916 (2014).
21. A. Messé, M. T. Hütt, C. C. Hilgetag, Toward a theory of coactivation patterns in excitable neural networks. *PLoS Comput. Biol.* **14**, e1006084 (2018).
22. M. Kaiser, C. C. Hilgetag, Optimal hierarchical modular topologies for producing limited sustained activation of neural networks. *Front. Neuroinform* **4**, 8 (2010).
23. S. J. Wang, C. C. Hilgetag, C. Zhou, Sustained activity in hierarchical modular neural networks: Self-organized criticality and oscillations. *Front. Comput. Neurosci.* **5**, 30 (2011).
24. P. Moretti, M. A. Munoz, Griffiths phases and the stretching of criticality in brain networks. *Nat. Commun.* **4**, 1–10 (2013).
25. C. Fretter, A. Lesne, C. C. Hilgetag, M. T. Hütt, Topological determinants of self-sustained activity in a simple model of excitable dynamics on graphs. *Sci. Rep.* **7**, 42340 (2017).
26. G. Zamora-López, C. Zhou, J. Kurths, Cortical hubs form a module for multisensory integration on top of the hierarchy of cortical networks. *Front. Neuroinf.* **4**, 1 (2010).
27. M. P. Van Den Heuvel, O. Sporns, Rich-club organization of the human connectome. *J. Neurosci.* **31**, 15775–15786 (2011).
28. M. P. van den Heuvel *et al.*, Abnormal rich club organization and functional brain dynamics in schizophrenia. *JAMA Psychiatry* **70**, 783–792 (2013).
29. W. J. Lee, C. E. Han, I. Aganj, S. W. Seo, J.- K. Seong, Distinct patterns of rich club organization in Alzheimer's disease and subcortical vascular dementia: A white matter network study. *J. Alzheim. Dis.* **63**, 977–987 (2018).
30. T. Yan *et al.*, Rich club disturbances of the human connectome from subjective cognitive decline to Alzheimer's disease. *Theranostics* **8**, 3237–3255 (2018).
31. Y. Wang *et al.*, Disrupted rich club organization and structural brain connectome in unmedicated bipolar disorder. *Psychol. Med.* **49**, 510–518 (2019).
32. H. Verhelst, C. Vander Linden, T. De Pauw, G. Vingerhoets, K. Caeyenberghs, Impaired rich club and increased local connectivity in children with traumatic brain injury: Local support for the rich?. *Hum. Brain Mapp.* **39**, 2800–2811 (2018).
33. H. Nakao, A. S. Mikhailov, Turing patterns in network-organized activator–inhibitor systems. *Nat. Phys.* **6**, 544–550 (2010).
34. M. Müller-Linow, C. C. Hilgetag, M. T. Hütt, Organization of excitable dynamics in hierarchical biological networks. *PLoS Comput. Biol.* **4**, e1000190 (2008).
35. J. G. Orlandi, J. Soriano, E. Alvarez-Lacalle, S. Teller, J. Casademunt, Noise focusing and the emergence of coherent activity in neuronal cultures. *Nat. Phys.* **9**, 582–590 (2013).
36. E. M. Izhikevich, G. M. Edelman, Large-scale model of mammalian thalamocortical systems. *Proc. Natl. Acad. Sci. U.S.A.* **105**, 3593–3598 (2008).
37. J. Lallouette, M. De Pittà, H. Berry, "Astrocyte networks and intercellular calcium propagation" in *Computational Glioscience*, M. De Pittà, H. Berry, Eds. (Spring Series in Computational Neuroscience, Springer, Cham, Switzerland, 2019), pp. 177–210.
38. M. Girvan, M. E. J. Newman, Community structure in social and biological networks. *Proc. Nat. Acad. Sci. U.S.A.* **99**, 7821–7826 (2002).
39. E. Berther, M. A. Porter, K. E. Daniels, Forecasting failure locations in 2-dimensional disordered lattices. *Proc. Nat. Acad. Sci. U.S.A.* **116**, 16742–16749 (2019).
40. P. Moretti, M. Zaiser, Network analysis predicts failure of materials and structures. *Proc. Nat. Acad. Sci. U.S.A.* **116**, 16666–16668 (2019).
41. M. Müller-Linow, C. Marr, M. Hütt, Topology regulates the distribution pattern of excitations in excitable dynamics on graphs. *Phys. Rev.* **74**, 016112 (2006).
42. M. Hütt, A. Lesne, Interplay between topology and dynamics in excitation patterns on hierarchical graphs. *Front. Neuroinform.* **3**, 28 (2009).
43. G. C. Garcia, A. Lesne, M. Hütt, C. C. Hilgetag, Building blocks of self-sustained activity in a simple deterministic model of excitable neural networks. *Front. Comput. Neurosci.* **6**, 50 (2012).
44. M. T. Hütt, M. Jain, C. C. Hilgetag, A. Lesne, Stochastic resonance in discrete excitable dynamics on graphs. *Chaos, Solit. Fractals* **45**, 611–618 (2012).
45. A. Messé, M. T. Hütt, P. König, C. C. Hilgetag, A closer look at the apparent correlation of structural and functional connectivity in excitable neural networks. *Sci. Rep.* **5**, 7870 (2015).
46. P. Hagmann *et al.*, Mapping the structural core of human cerebral cortex. *PLoS Biol.* **6**, e159 (2008).
47. O. Sporns, The human connectome: A complex network. *Ann. N. Y. Acad. Sci.* **1224**, 109–125 (2011).
48. J. A. Roberts *et al.*, The contribution of geometry to the human connectome. *Neuroimage* **124**, 379–393 (2016).
49. M. D. Schirmer *et al.*, Rich-club organization: An important determinant of functional outcome after acute ischemic stroke. *Front. Neurol.* **10**, 956 (2019).
50. S. C. de Lange *et al.*, Shared vulnerability for connectome alterations across psychiatric and neurological brain disorders. *Nat. Hum. Behav.* **3**, 988–998 (2019).
51. A. Díaz-Parra, Z. Osborn, S. Canals, D. Moratal, O. Sporns, Structural and functional, empirical and modeled connectivity in the cerebral cortex of the rat. *Neuroimage* **159**, 170–184 (2017).
52. T. W. Lee, S. W. Xue, Revisiting the functional and structural connectivity of large-scale cortical networks. *Brain Connect.* **8**, 129–138 (2018).
53. A. Messé, Parcellation influence on the connectivity-based structure–function relationship in the human brain. *Hum. Brain Mapp.* **41**, 1167–1180 (2020).
54. Y. Qian, X. Huang, G. Hu, X. Liao, Structure and control of self-sustained target waves in excitable small-world networks. *Phys. Rev.* **81**, 036101 (2010).
55. X. H. Liao *et al.*, Oscillation sources and wave propagation paths in complex networks consisting of excitable nodes. *Front. Phys.* **6**, 124–132 (2011).
56. G. C. Garcia, A. Lesne, C. C. Hilgetag, M. T. Hütt, Role of long cycles in excitable dynamics on graphs. *Phys. Rev.* **90**, 052805 (2014).
57. H. Nakao, A. S. Mikhailov, Turing patterns in network-organized activator-inhibitor systems. *Nat. Phys.* **6**, 544–550 (2010).
58. C. Seguin, A. Razi, A. Zalesky, Send-receive communication asymmetry in brain networks: Inferring directionality of neural signalling from undirected structural connectomes. bioRxiv:10.1101/573071 (14 August 2019).
59. S. N. Dorogovtsev, A. V. Goltsev, J. F. F. Mendes, Critical phenomena in complex networks. *Rev. Mod. Phys.* **80**, 1275–1335 (2008).
60. M. A. Muñoz, Colloquium: Criticality and dynamical scaling in living systems. *Rev. Mod. Phys.* **90**, 031001 (2018).
61. A. Haimovici, E. Tagliazucchi, P. Balenzuela, D. R. Chialvo, Brain organization into resting state networks emerges at criticality on a model of the human connectome. *Phys. Rev. Lett.* **110**, 178101 (2013).
62. P. Villegas, P. Moretti, M. A. Muñoz, Frustrated hierarchical synchronization and emergent complexity in the human connectome network. *Sci. Rep.* **4**, 5990 (2014).
63. A. Safari, P. Moretti, M. A. Muñoz, Topological dimension tunes activity patterns in hierarchical modular networks. *New J. Phys.* **19**, 113011 (2017).
64. M. Boguná, C. Castellano, R. Pastor-Satorras, Nature of the epidemic threshold for the susceptible-infected-susceptible dynamics in networks. *Phys. Rev. Lett.* **111**, 068701 (2013).
65. S. V. Buldyrev, R. Parshani, G. Paul, H. E. Stanley, S. Havlin, Catastrophic cascade of failures in interdependent networks. *Nature* **464**, 1025–1028 (2010).
66. F. Morone, K. Roth, B. Min, H. E. Stanley, H. A. Makse, Model of brain activation predicts the neural collective influence map of the brain. *Proc. Natl. Acad. Sci. U.S.A.* **114**, 3849–3854 (2017).
67. L. Hufnagel, D. Brockmann, T. Geisel, Forecast and control of epidemics in a globalized world. *Proc. Natl. Acad. Sci. U.S.A.* **101**, 15124–15129 (2004).
68. D. Brockmann, D. Helbing, The hidden geometry of complex, network-driven contagion phenomena. *Science* **342**, 1337–1342 (2013).
69. R. Cohen, S. Havlin, D. Ben-Avraham, Efficient immunization strategies for computer networks and populations. *Phys. Rev. Lett.* **91**, 247901 (2003).
70. Y. Chen, G. Paul, S. Havlin, F. Liljeros, H. E. Stanley, Finding a better immunization strategy. *Phys. Rev. Lett.* **101**, 058701 (2008).
71. S. Pei, H. A. Makse, Spreading dynamics in complex networks. *J. Stat. Mech. Theor. Exp.* **2013**, P12002 (2013).
72. A. V. Goltsev, S. N. Dorogovtsev, J. G. Oliveira, J. F. F. Mendes, Localization and spreading of diseases in complex networks. *Phys. Rev. Lett.* **109**, 128702 (2012).
73. R. Pastor-Satorras, C. Castellano, Distinct types of eigenvector localization in networks. *Sci. Rep.* **6**, 18847 (2016).